Available online at www.sciencedirect.com
SCIENCE DIRECT
Minerals Engineering 19 (2006) 505–514
MINERALS ENGINEERING
This article is also available online at: www.elsevier.com/locate/mineng

Laboratory evaluation of Fe^0 barriers to treat acidic leachates

Georgios Bartzas [a], Kostas Komnitsas [b,*], Ioannis Paspaliaris [a]

[a] School of Mining and Metallurgical Engineering, National Technical University of Athens, 157 80 Athens, Greece
[b] Department of Mineral Resources Engineering, Technical University Crete, University Campus, Akrotiri, 73100 Chania, Greece

Received 8 August 2005; accepted 11 September 2005
Available online 2 November 2005

Abstract

In the present study, flow-through column experiments using a series of continuous-flow columns were conducted to investigate the performance of Fe^0 permeable reactive barriers (PRB) for the treatment of acidic leachates generated in active or abandoned mining and waste disposal sites. Simulated AMD solutions of low and high metal ion concentration were pumped at different flow rates into the laboratory system. Concentration profiles under steady-state transport conditions were developed by measuring metal ion concentration at various sampling ports. Results show that metal ion removal is mainly accomplished via redox reactions that initiate precipitation of mineral phases. Sulfate green rust was identified from the analysis of precipitates formed on the iron surface; sulfate and heavy metals uptake by green rust is a secondary clean up mechanism. Experimental results as well as geochemical modeling by PHREEQC-2 indicate that cadmium and copper are removed by redox reactions while aluminum, manganese, nickel, cobalt and zinc are mainly removed as metal hydroxides. It is therefore seen than zero-valent iron barriers can be used as an environmentally and economically viable remediation technology for the clean up of acidic leachates loaded with several inorganic contaminants and sulfates and the subsequent prevention of groundwater contamination.

Keywords: Acid rock drainage; Leaching; Environmental

1. Introduction

Acid mine drainage (AMD), a result of oxidation of residual sulphide minerals (mainly pyrite) upon exposure to water and oxygen, continues to be an important worldwide source of surface and groundwater contamination associated with active or abandoned mining and waste disposal sites. The complete reaction of pyrite oxidation can be summarized by the following equation:

$$4FeS_2(s) + 15O_2 + 14H_2O \Rightarrow 4Fe(OH)_3(s) + 8SO_4^{2-} + 16H^+ \quad (1)$$

Thus, AMD is usually characterized by low pH and high concentration of sulfate, iron, and heavy metals which can severely contaminate surface and groundwater, as well as soil (Kontopoulos et al., 1995).

Conventional techniques for controlling or treating AMD involve mainly the use of active systems by adding alkaline materials that produce large volumes of metal-rich sludge and often require long-term operating costs. In case groundwater is impacted pump and treat seems to be the only well established technology; its cost though is considered extremely high in case huge volumes of groundwater have to be cleaned up. The use of permeable reactive barriers (PRBs) composed of reactive media and installed across the flow path of the contaminated plume offers a relatively low-cost alternative to traditional pump and treat (Gavaskar et al., 1998).

Zero valent iron (Fe^0) is quite effective for the clean up of groundwater or leachates containing chlorinated organic compounds or inorganic contaminants. Recent studies have shown that Fe^0 removes effectively several inorganic contaminants such as arsenic, chromium, uranium and selenium

* Corresponding author. Tel.: +30 28210 37686; fax: +30 28210 69554.
E-mail addresses: gbartzas@metal.ntua.gr (G. Bartzas), komni@mred.tuc.gr (K. Komnitsas), paspali@metal.ntua.gr (I. Paspaliaris).

0892-6875/$ - see front matter © 2005 Elsevier Ltd. All rights reserved.
doi:10.1016/j.mineng.2005.09.032

from aqueous solutions (Cantrell et al., 1995; Su and Puls, 2001; Alowitz and Scherer, 2002; Zhang et al., 2005). However, only a few studies have addressed issues related to acidic leachates treatment (Shokes and Möller, 1999; Wilkin and McNeil, 2003). Possible removal mechanisms include direct electron exchange between a contaminant (e.g. chromium) and Fe^0 that is oxidized to ferrous or ferric and adsorption onto the surface of iron particles or onto iron corrosion products formed on the non-reacted metal surface. Recent studies have shown that microbial activity can also enhance reductive treatment (Gu et al., 2002).

Most experimental studies conducted to date for the treatment of acidic leachates using Fe^0 have been mainly restricted to batch systems. Although these studies provide useful information regarding metal removal mechanisms, there is still a gap of knowledge concerning the long-term performance of Fe^0 barriers. Therefore, in this experimental study, laboratory columns were set up and operated under conditions simulating those anticipated in the field.

The objectives of this study were (a) to investigate the feasibility of Fe^0 barriers for the removal of several hazardous metallic ions from acidic leachates generated in mining and waste disposal sites, (b) to elucidate the geochemical mechanisms that control the system and (c) to assess the long-term performance of such systems. Particular emphasis was given on the ability of Fe^0 to remove low and high concentrations of toxic metals under different flow conditions, such as those anticipated in field installations.

2. Experimental methodology

2.1. Materials

Iron filings: Zero-valent iron filings (0.2–1.2 mm) were obtained as cast iron grit from Gotthart Maier Mettallpulver GmbH, Germany and used as received. They contain 92% elemental iron with small amounts of other metals (<2% Si, <1% Cu, and <1% Mn) and ~3.3% carbon. Their specific surface area as determined by the BET N_2-method was 0.0482 m^2/g. This value is comparable to values of commercial and non-commercial Fe^0 filings used in other studies as seen in Table 1.

Mineralogical analysis carried out by XRD and SEM revealed the presence of elemental iron, graphite and iron oxides. Fig. 1 shows the shape, the particle size and the rough surface of the iron filings.

Silica sand: The silica sand (0.2–1.0 mm) used originates from a coastal area of Milos island, Greece. Its chemical analysis shows that it contains about 97% SiO_2 and traces of aluminum and sodium oxides as well as of other minerals. No iron oxides were detected. The sand was soaked prior to use in 8% v/v HNO_3 for 24 h and then rinsed with deionized water.

2.2. Column studies

The experimental procedure (design, column set-up and operation) was similar to that described in an earlier publication (Komnitsas et al., 2004). Briefly, two plexiglas columns (45 cm length, 5 cm internal diameter) placed in a series were used. Each column was homogenously packed with a 40 cm layer of 50:50 w/w iron filings:silica sand in the middle and 2.5 cm layers of silica sand in both ends. The total pore volume was determined by pumping a known volume of distilled water through the dry columns and collecting the effluent; the difference is the total column pore volume (863 mL). The pore volume was also measured by tracer tests (data not shown) and was found to be on average 858 mL. The initial porosity of the medium (0.55) was determined by using the following equation.

$$p = 1 - \frac{\rho_{bulk}}{(spg_{Fe^0/sand} \times \rho_{H_2O})} \quad (2)$$

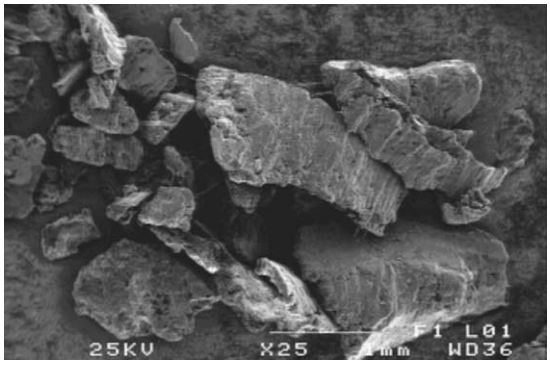

Fig. 1. SEM image showing the shape, the grain size and the rough surface of iron filings.

Table 1
Average specific surface area[a] of Fe^0 filings[b]

	Specific surface area (m^2/g)	Iron content (%)	References
Aldrich powder	0.094	97	Miehr et al. (2004)
Master builders	1.2	–	Westerhoff (2003)
Connelly	1.68	90	Alowitz and Scherer (2002)
Fisher filings	0.091–0.05	>97	Su and Puls (1999), Wilkin and McNeil (2003)
Fluka filings	0.229	+99	Miehr et al. (2004)
Peerless filings	0.87–3.05	>90	Lee et al. (2004), Miehr et al. (2004), Wilkin and McNeil (2003)
Baker chips	0.016	–	Westerhoff (2003)
Merck powder	0.1	99.9	Astrup et al. (2000)

[a] Determined by the BET method.
[b] Used as received but some samples were sieved to obtain specific fractions.

where ρ_{H_2O} is the density of water at 25 °C, $spg_{Fe^0/sand}$ is the specific gravity at 25 °C (4.58), and ρ_{bulk} is the bulk density of the Fe^0/sand mixture (2.07 g/cm^3). Column porosity was also determined by a tracer test experiment. Non-reactive chloride was flushed into the column and the breakthrough of the tracer front was measured at the effluent sampling port. The experimental data were modelled with the one dimensional advection–dispersion equation and the same porosity value was determined.

Experiments were performed at constant temperature, 25 ± 2 °C. Artificial AMD solutions with low and high metal ion concentration were prepared in HCl-cleaned glassware by dissolving the salts seen in Table 2 in deionized water. The quality of the artificial AMD prepared is based on the results of a USEPA survey as well as a study of the Department of Environmental Protection in Pennsylvania for acid-producing coal mine waters (USEPA, 1976; Brady et al., 1998). All chemicals were reagent grade from Merck, Aldrich or Fluka and used as received.

A peristaltic pump (Gala 4-W) was used to pump the artificial AMD from a collapsible teflon bag through the columns at two desirable (low and high) flow rates. In order to eliminate channelling and gas entrainment, the upflow mode was applied. Before starting the tests at steady conditions, three pore volumes of distilled water were flushed through the columns to equilibrate the system and remove residual oxygen from the voids.

Modeling was performed within the Fe^0 PRB systems with the computer program PHREEQC-2 (Parkhurst and Appelo, 1999) for speciation and one dimensional transport. Model simulations predicted the formation of solution complexes, precipitation of solid phases and sorption onto newly formed iron oxide phases. Thermodynamic constants were retrieved from the WATEQ4F database (Ball and Nordstrom, 1991).

2.3. Sampling and analytical methods

The columns were fitted with side ports installed along the walls at a distance of 20 cm (sampling port A) and 60 cm (sampling port B) from the inlet that allowed for regular sampling and determination of leachates quality during operation. Samples were also taken from the outlet of the second column (sampling port C). Head-space free aqueous samples were withdrawn from each sampling port very carefully to avoid disturbance using glass syringes as well as from the effluent and analyzed for pH and redox potential (E_h) immediately after sampling with a pH/Conductivity meter (Metrohm 691 pH meter). Solutions were filtered through 0.45 μm filters (Gelman Science sterile aerodisc), acidified and if necessary kept at 4 °C and then analyzed for Fe, Zn, Mn, Al, Ni, Cu, Co and Cd by flame atomic absorption spectrophotometry (Perkin Elmer 2100). Sulfate concentration was measured gravimetrically while ferrous iron concentration was determined by the 1,10-phenanthroline method.

Non-reacted Fe^0 and representative samples of exhausted reactive mixture were analyzed by X-ray diffraction (XRD) with a Siemens D 5000 diffractometer using Cu Kα radiation. These samples were also examined with a JEOL scanning electron microscope (SEM). DIFFRAC-AT software was used to analyze the XRD patterns and determine all mineralogical phases present.

Table 2
Artificial AMD solutions composition and corresponding chemicals

Contaminants	Concentration in mg/l		Used chemicals
	Low (LC)	High (HC)	
Al^{3+}	100	500	$Al_2(SO_4)_3 \cdot 18H_2O$
Zn^{2+}	20	100	$ZnSO_4 \cdot 7H_2O$
Cd^{2+}	5	25	$3CdSO_4 \cdot 8H_2O$
Cu^{2+}	5	50	$CuSO_4 \cdot 5H_2O$
Mn^{2+}	5	50	$MnSO_4 \cdot H_2O$
Ni^{2+}	5	50	$NiSO_4 \cdot 6H_2O$
Co^{2+}	5	50	$CoSO_4 \cdot 7H_2O$
SO_4^{2-}	1345	5840	–
pH	1.8	2.2	

2.4. Column transport parameters

The slow flow rate (SF) and fast flow rate (FF) columns were operated continuously at flow rates of 13.7 and 68.5 ml/h, respectively. These correspond to average Darcy velocities of 30.48 and 152.4 cm/day which are similar with those reported in literature (6–220 cm/day) for field zero-valent iron PRB installations (Phillips et al., 2000; Morkin et al., 2000). The slow flow rate represents a typical field groundwater velocity (Domenico and Schwartz, 1998). The fast flow rate allows for faster prediction of aqueous-solid phase compositional changes and equilibrium (e.g. precipitation, dissolution, adsorption and desorption). Therefore, the pumping rates used simulate 2 and 10 years of flow through a field permeable barrier installation respectively.

3. Results and discussion

Presentation and discussion of results focuses mainly on the slow-flow rate column system, where experimental data are not affected to a great extent by heterogeneity as in the fast-flow rate column system. Although the fast-flow rate column system allows for more frequent sampling and analysis with less impact on column flow, it is anticipated that microbial activity and secondary precipitation will primarily occur in the slow-flow rate columns due to their higher residence times. In addition, slow-flow columns provide baseline conditions for comparison with the accelerated ones as well as with previous similar studies.

3.1. Column studies

Solute transport through each column is expressed as normalized concentration (C/C_0) versus normalized time (number of pore volumes), where C is the effluent

concentration and C_0 is the average influent concentration over the entire experimental duration. Slow flow-rate columns were run at 13.7 ml/h, with about 39 h residence time over different time periods in which 32 and 19 pore volumes of low and high load simulated AMD were pumped, respectively. Nearly 27.6 l and 16.4 l of low and high loads of acidic leachates were treated with 1050 g of Fe^0/sand mixture contained in each column, respectively. The operation was ceased when the formation of precipitates (corrosion products) close to sampling port A prohibited free solution flow.

pH, E_h and iron corrosion. Fig. 2a and b present the results for pH and E_h variation in the low concentration slow-flow rate (LCSF) and high concentration slow-flow rate (HCSF) columns, respectively.

Once the highly acidic feed reacts with the Fe^0 fillings, pH increases and E_h decreases as a result of iron dissolution

$$Fe^0 + 2H_2O \Rightarrow Fe^{+2} + H_2 + 2OH^- \quad (3)$$

The effluent pH increases to about 8.5 in the LCSF and 5.8 in the HCSF column from its initial values of 2.2 and 1.8 respectively. It is clear from the experimental results that the principal mechanism for E_h decrease and pH increase is the dissolution of iron. These changes became gradually less dramatic suggesting that Fe^0 particles undergo some degree of passivation due to precipitation of secondary phases at sampling port A after 15 pore volumes (pH rise). E_h drops sharply since zero-valent iron is a strong electron donor. Geochemical conditions in both columns confirm that the environment becomes over time strongly reducing, causing thus the redox front to move upwards.

Total iron concentration in the LCSF column increased sharply and reached steady-state conditions after 24 pore volumes (Fig. 3a). On the contrary, total dissolved iron in the HCSF column increased gradually to reach the maximum concentration after seven pore volumes and then decreased rapidly indicating signs of actual Fe^0 exhaustion (Fig. 3b). Effluent measurements at the end of the run showed that almost 80% and 92% of the total dissolved iron was present in its ferrous state in the LCSF and HCSF column system, respectively.

PHREEQC-2 indicates that the corrosion of Fe^0 and the increase of pH may cause precipitation of $Fe(OH)_2$ at the start of the process

$$Fe^0 + 2H_2O \Rightarrow Fe(OH)_2 + 2H^+ + 2e^- \quad (4)$$

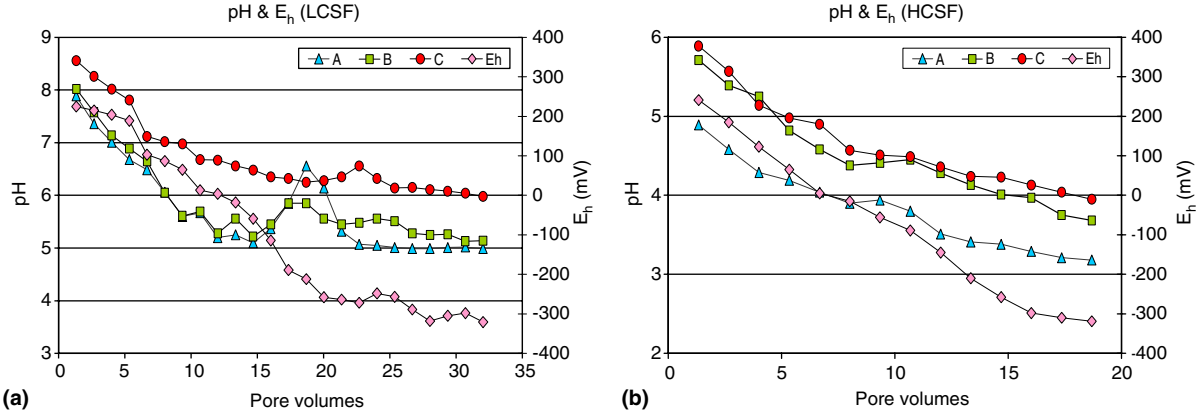

Fig. 2. (a) and (b) pH at sampling ports A–C and E_h at sampling port C versus pore volumes in the LCSF and HCSF column systems.

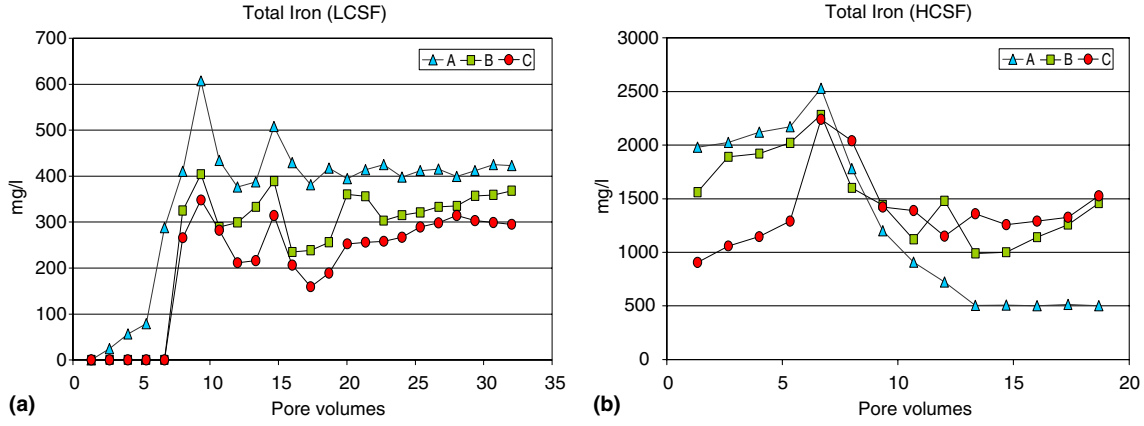

Fig. 3. (a) and (b) total dissolved iron versus pore volumes in the LCSF and HCSF column systems.

In reduced conditions, the freshly precipitated $Fe(OH)_2$ is stable but thermodynamically can be converted to either magnetite or intermediate products as seen in the following reactions:

$$3Fe(OH)_2 \Rightarrow Fe_3O_4 + H_2 + 2H_2O + 2e^- \quad (5)$$

$$6Fe(OH)_2 + SO_4^{2-} + 2H_2O \Rightarrow [Fe_4^{2+}Fe_2^{3+}(OH)_{12}][SO_4 \cdot 2H_2O] + 2e^- \quad (6)$$

Sulfate green rust $[GR(SO_4^{2-})]$ consists of alternating positively charged brucite-like iron hydroxide layers $[Fe_4^{2+}Fe_2^{3+}(OH)_{12}]^{2+}$ due to the presence of Fe^{3+} cations and negatively charged interlayers of anions $[SO_4 \cdot 8H_2O]^{2-}$ that maintain the whole electroneutrality (Génin et al., 1996). $GR(SO_4^{2-})$ as an intermediate product often transforms during the hydrolytic oxidation of Fe^{2+} to FeOOH (Olowe and Génin, 1991). Depending on the rate of iron oxidation green rust may also convert to goethite (a–FeOOH), lepidocrocite (g–FeOOH), maghemite (Fe_2O_3), or magnetite (Fe_3O_4) (Furukawa et al., 2002).

Although PHREEQC-2 simulations predict the formation of all previously mentioned Fe^0 corrosion products (with the exception of green rust), hematite and/or magnetite were the only products detected under the present experimental conditions. This is in agreement with previous studies (Cornell and Schwertmann, 1996) which also suggest that the direct precipitation of Fe corrosion products is possible.

Gradually, an oxide film formed by the oxidation of zero-valent iron covers its surface and subsequently reduces the overall reactivity of the system (Wang and Zhang, 1997). However, in the present study, it seems that this oxide layer is either not formed or is immediately dissolved by the inflowing acidic solution.

Sulfate. Sulfate is the predominant anion in acidic mine waters and leachates as well as in the simulated solutions used in the present study. Previous studies showed that its chemical interaction with forms of iron and aluminum plays a central role in the solubility, speciation, toxicity and removal of these and other associated ions (Satapanajaru et al., 2003). Fig. 4 shows the concentration profiles of sulfate removal. The low and high initial sulfate concentration used was 1.34 and 5.84 g l^{-1} respectively. The sulfate concentration in the final effluent, after its reaction with the iron fillings, was significantly lower (0.58 g l^{-1}) for the LCSF and slightly lower (3.28 g l^{-1}) for the HCSF column system.

The reduction of sulfate by zero-valent iron can be expressed by the following direct reaction:

$$4Fe^0 + SO_4^{-2} + 9H^+ \Rightarrow 4Fe^{+2} + HS^- + 4H_2O \quad (7)$$

This reaction consumes much more Fe^0 compared with the quantity consumed by reduction and precipitation of each individual metal (e.g 50 times more for Cr reduction) (Mayer, 1999). Geochemical modelling with PHREEQC-2 also confirms that the major contribution to iron corrosion is due to sulfate reduction. However, sulfate may be

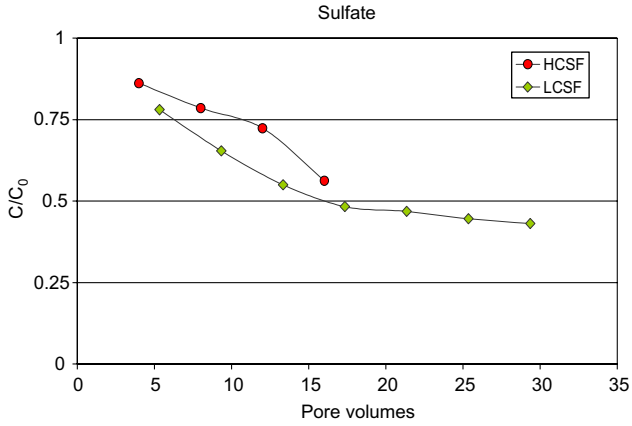

Fig. 4. Effluent sulfate breakthrough curves versus pore volumes in the HCSF and LCSF column systems.

removed from solution by precipitation as metal sulfur compound, e.g., metal sulphate/hydroxide complexes.

As the acidic AMD solution percolates through the column system, the "precipitation front" is initially seen as a dark green boundary, mainly because of the presence of sulfate green rust, $GR(SO_4^{2-})$, as Fe^0 oxidises to Fe^{2+}. At the end of the experiment the precipitation front is red, as Fe^{2+} converts to Fe^{3+}. The higher rate of SO_4^{2-} removal seen for the first 17 pore volumes in the LCSF column system indicates the formation of $GR(SO_4^{2-})$ due to the oxidation of Fe^0 to $Fe^{2+}$and Fe^{3+} (Eqs. (3)–(5)). In addition, it is seen that the decrease of dissolved sulfate concentration in both columns is in the same order of magnitude as the increase of dissolved iron, fact that also suggests the formation of $GR(SO_4^{2-})$. The results regarding sulphate removal, however, do not agree with data from field applications where sulfate is in general completely removed from acidic mine waters and groundwater plumes (Gu et al., 2002). This difference is probably due to the microbial activity of sulfate-reducing bacteria which is often noticed in field installations (Phillips et al., 2000; Gu et al., 2002) but is rarely seen in laboratory studies. However, in the present study microbial activity was evident in the lower parts of the LCSF column towards the end of the experiment, as seen in the SEM image, where rod shaped sulphate reducing bacteria are seen (Fig. 5). Another explanation of this discrepancy may be also due to the following reactions describing the mechanisms that control geochemistry in the field

$$4Fe^0 + 8H_2O \Rightarrow 4Fe^{+2} + 8OH^- + 4H_2 \quad (8)$$

$$SO_4^{-2} + 4H_2 \Rightarrow HS^- + 3H_2O + OH^- \quad (9)$$

$$4Fe^{2+} + HS^- + 7OH^- \Rightarrow FeS(am) + 3Fe(OH)_2(am) + H_2O \quad (10)$$

It is important to note that high concentration of sulfates in the contaminated plume is not expected to cause increased iron corrosion in field applications due to the activity of sulfate-reducing bacteria as previously mentioned.

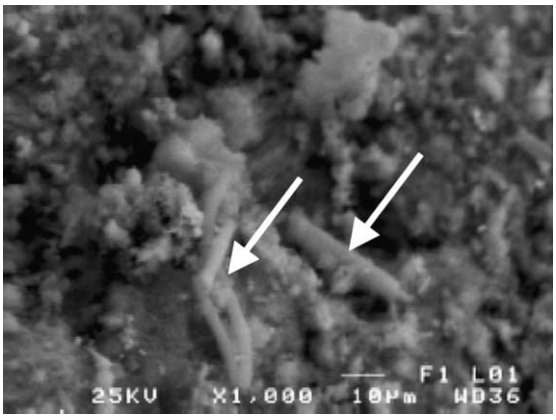

Fig. 5. SEM image of microbial activity within the LCSF column system.

Aluminum. Al concentration in both columns was maintained at or below detection limits (0.65 mg/l) at sampling ports B and C throughout the experimental period, while at sampling port A in the LCSF column system started to increase slightly after 20 pore volumes (Fig. 6a) and reached or exceeded its high feed value in the HCSF column system (Fig. 6b) after 13 pore volumes.

Geochemical calculations using the PHREEQC-2 software predict that aluminum concentration, when pH is above or below 5.5, is determined by the formation of amorphous $Al(OH)_3$ or jurbanite ($AlOHSO_4 \cdot 5H_2O$) respectively. This prediction is supported by the relatively low sulfate concentration recorded at the final effluents of both columns as well as by previous studies (Shokes and Möller, 1999; Wilkin and McNeil, 2003).

Copper and Cadmium. Cu and Cd were removed below detection limits (i.e. 0.05 mg/l and 0.02 mg/l, respectively) in the effluent port of the simulated LCSF column system (Figs. 7a and 8a). Copper is easily subject to reduction through the oxidation of Fe^0 as seen in the following reaction:

$$Fe^0 + Cu^{2+} \iff Cu^0 + Fe^{2+} \quad (11)$$

The main mechanism for fast removal of Cu^{2+} ions by Fe^0 is cementation (Khudenko, 1987) or reductive precipitation (Blowes et al., 2000). Recent studies suggest also the ability of the precipitated GR(SO_4^{2-}) to reduce Cu^{2+} under iron-reducing conditions (O'Loughlin et al., 2003).

In the presence of high Cu^{2+} concentration (HCSF column), the reduction of Cu^{2+} to Cu^0 by Fe^0 results in

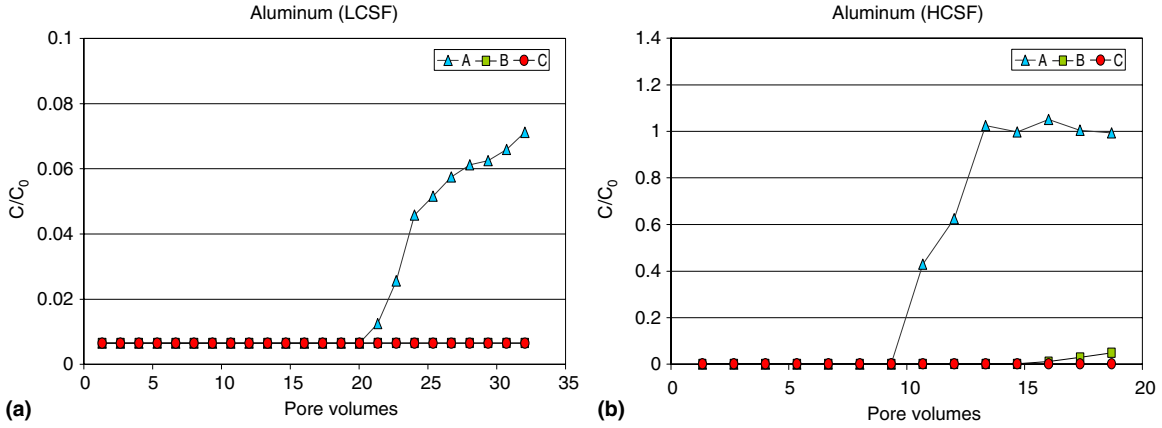

Fig. 6. (a) and (b) aluminum breakthrough curves at sampling ports A, B and C versus pore volumes in the LCSF and HCSF column systems.

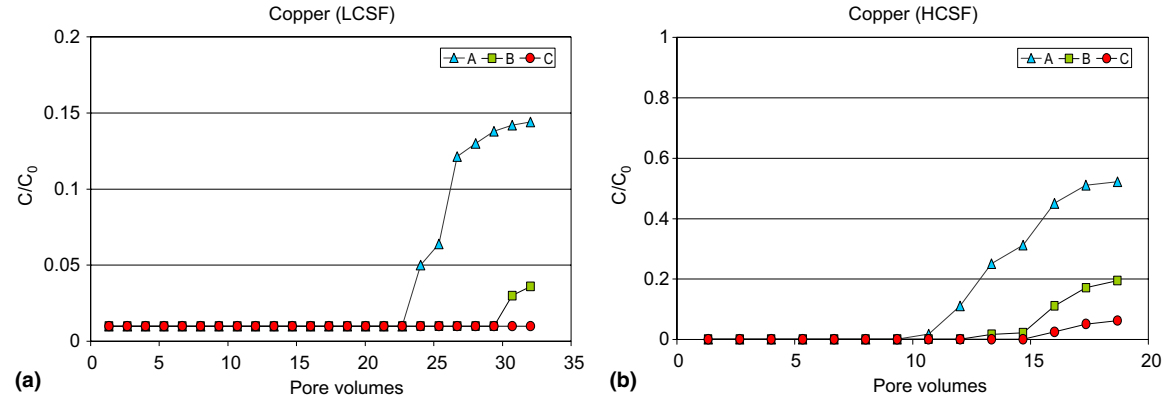

Fig. 7. (a) and (b) copper breakthrough curves at sampling ports A, B and C versus pore volumes in the LCSF and HCSF column systems.

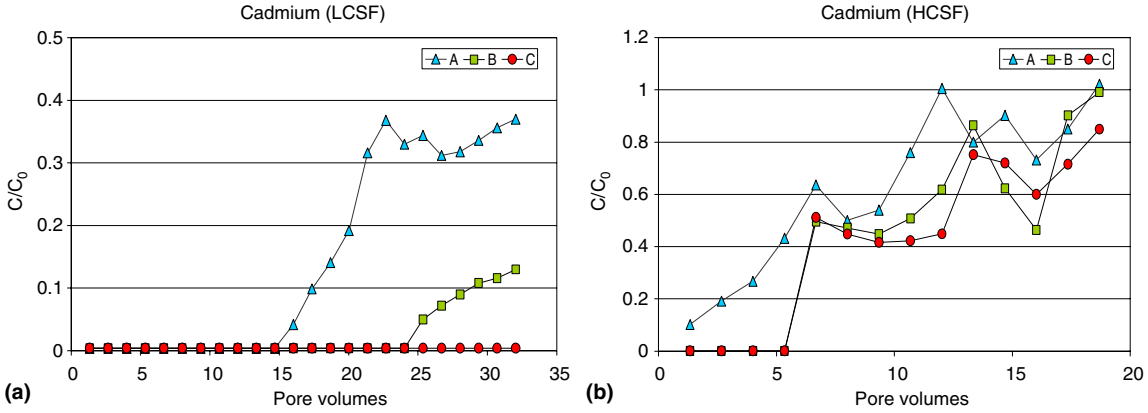

Fig. 8. (a) and (b) cadmium breakthrough curves at sampling ports A, B and C versus pore volumes in the LCSF and HCSF column systems.

significant plating of the iron surface by copper metal and further elimination of the active iron surface sites due to chemical armouring. Signs of iron exhaustion were seen after 15 pore volumes.

Cadmium exhibited nearly similar behaviour to copper suggesting that for both metals the same clean up mechanism takes place. Measurements at sampling ports A and B in the LCSF column system (Fig. 8a) show that Cd concentration is maintained at or below detection limits over a long period (after 15 and 24 pore volumes respectively). Cd concentration at sampling port A reached nearly half of its initial value after almost 8 weeks of operation, while the effluent concentration remained extremely low even after 12.5 weeks. Geochemical modelling with PHREEQC-2 predicts that at alkaline pH both Cu and Cd concentration appears to be controlled by the solubility of CuO and $Cd(OH)_2$ respectively.

Manganese. The significantly increased concentration of dissolved Mn in sampling port A in both columns suggests that no clean up activity is seen in the lower parts of the system (Fig. 9a and b). However signs of Mn removal are seen at sampling ports B and C in both columns during the early stages of operation. The elevated final Mn concentration in both columns is due to re-dissolution of relatively unstable precipitates formed at earlier stages by the action of the fresh acidic feed or desorption of Mn from the zero-valent iron particles. Moreover, the increased concentration of Mn in the LCSF column system effluent, compared with those measured in sampling ports A and B, may be also due to preferential flow of solution (tracer tests).

Similar phenomena were also observed in other laboratory scale studies using zero-valent iron or other reactive media (Park et al., 2002; Kamolpornwijit et al., 2003; Komnitsas et al., 2004). PHREEQC-2 simulation predicts that the concentration of dissolved Mn along the column profile is mainly determined by the precipitation of pyrocroite $Mn(OH)_2(am)$ which is relatively insoluble and precipitates at early stages when pH still remains at alkaline or neutral regions. Possible Mn sinks due to $Mn(OH)_2$ formation are also mentioned in previous studies (Wilkin and McNeil, 2003).

Zinc. Dissolved Zn concentration in both columns is maintained at low values at sampling ports B and C (<0.1% of the initial concentration) throughout the experimental period (Fig. 10a and b). The concentration of Zn remains below detection limit at sampling port A in the LCSF column system after 20 pore volumes and then increases rapidly reaching breakthrough ($C/C_0 = 0.5$) after 32 pore volumes.

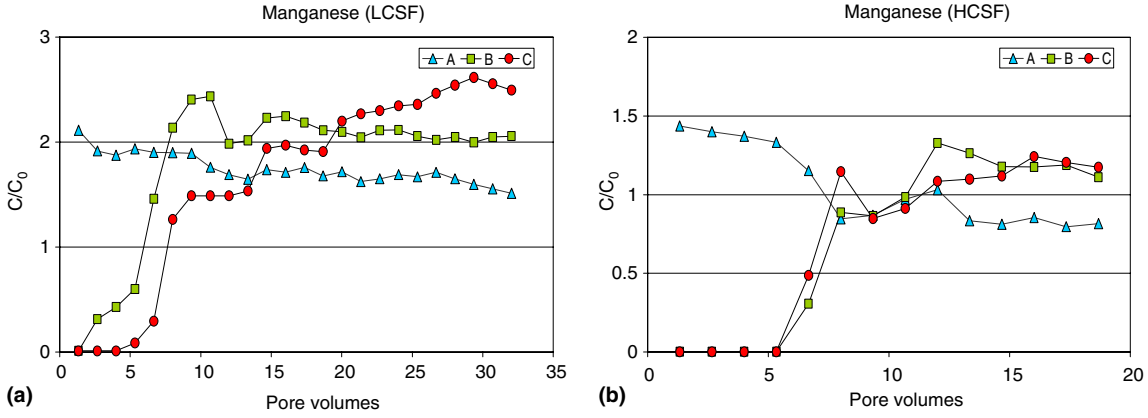

Fig. 9. (a) and (b) manganese breakthrough curves at sampling ports A, B and C versus pore volumes in the LCSF and HCSF column systems.

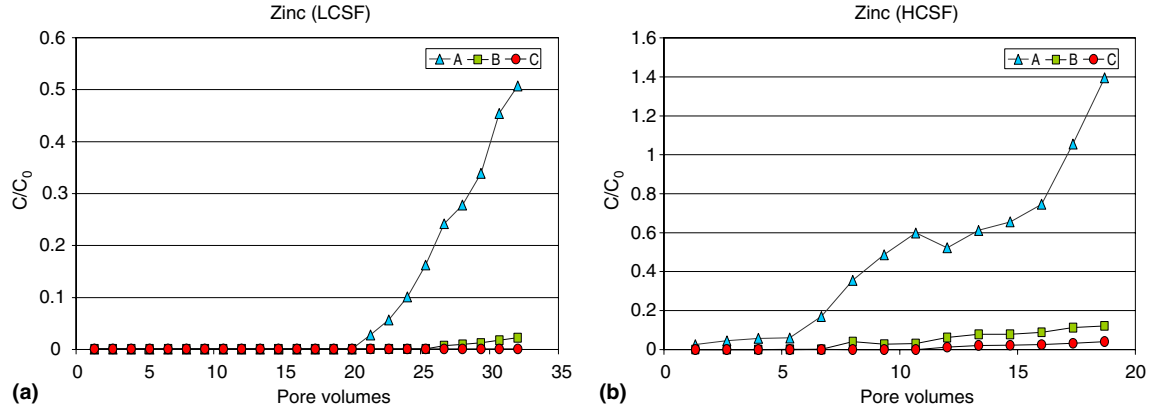

Fig. 10. (a) and (b) zinc breakthrough curves at sampling ports A, B and C versus pore volumes in the LCSF and HCSF column systems.

Under the acidic conditions used in this study, zinc does not seem to be absorbed onto the oxide layer (e.g ferrihydrite) formed on the surface of the zero-valent iron particles, as mentioned in previous studies (Wilkin and McNeil, 2003). Geochemical modelling predicts that $Zn(OH)_2$ precipitation controls Zn concentration in leachates (Herbert, 2003).

Cobalt and Nickel. As expected, cobalt and nickel show similar behaviour (Fig. 11). Both dissolved metal concentrations reached their initial value at sampling port A of the LCSF column system after 32 pore volumes whereas no cobalt or nickel were detected in the effluent of the same system over the entire experimental period.

As seen in Fig. 11b and d the efficiency of Fe^0 in removing these specific heavy metal ions from solution at high concentrations is limited. PHREEQC-2 predicts precipitation of nickel hydroxide at pH values greater than 7.5.

3.2. Hydrogen gas production

Hydrogen gas may be produced as a result of the electrolysis of water by iron (Eq. (3)). Throughout the

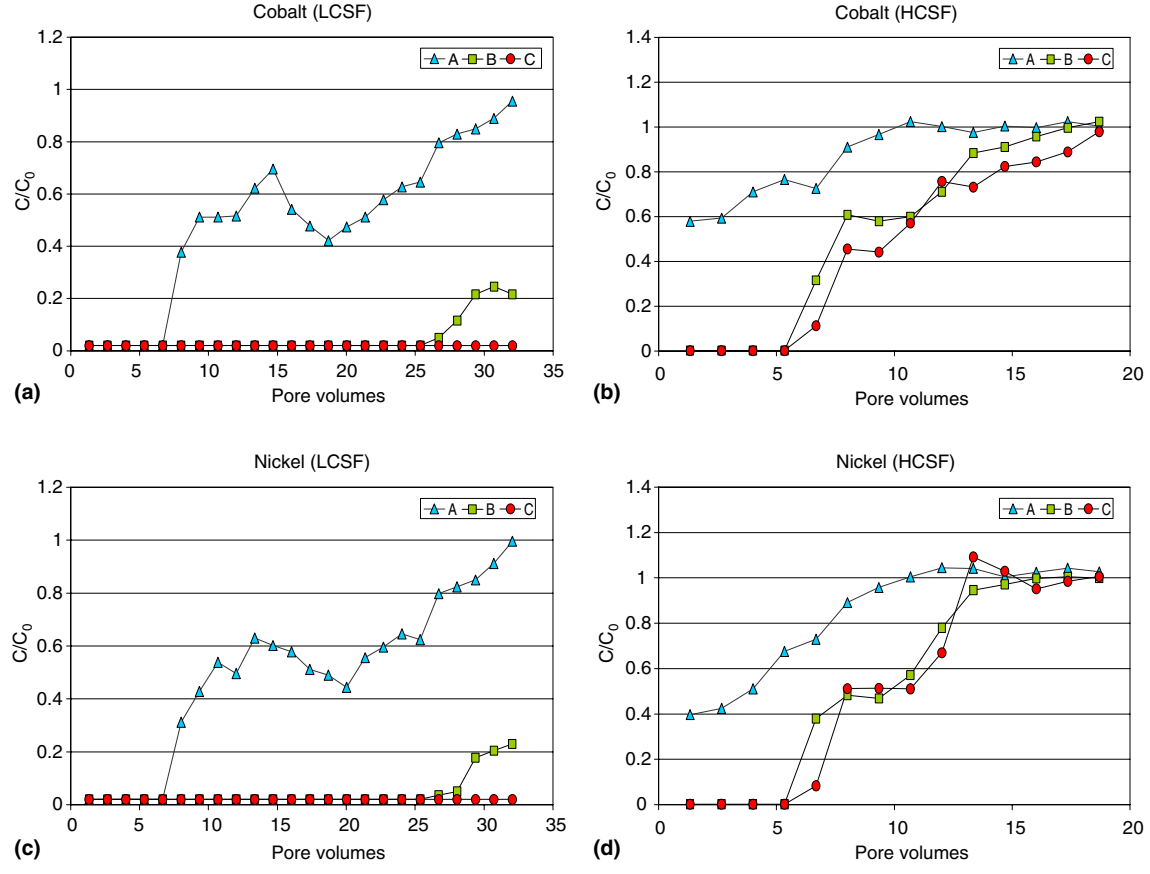

Fig. 11. Cobalt (a) and (b) and nickel (c) and (d) breakthrough curves at sampling ports A, B and C versus pore volumes in the LCSF and HCSF column systems.

experiments though no gas bubbles were seen in the mixed iron-sand packed columns in contrast to what is mentioned in previous studies (Kamolpornwijit et al., 2003). This may be due to the use of an iron-sand bed under flow conditions that minimize the production of hydrogen gas. Furthermore, it can be assumed that dissolved hydrogen gas produced by Fe^0 corrosion is consumed by other reduction reactions (e.g sulfate) (Eq. (9)) or by bacteria that act as electron donors. Previous studies mention that the production of gas bubbles disturbs plug flow characteristics and causes the development of preferential flow paths (Kamolpornwijit et al., 2003). Tracer tests through performed during column operation as well as visual observations do not confirm this effect.

3.3. Mineralogy

XRD analysis of exhausted zero-valent iron samples collected from the first, middle and last part of each column at the end of the test indicates that the main phases present are sulphate green rust in the LCSF (Fig. 12) and magnetite in the HCSF column system. GR(SO_4^{2-}) gives rise to a pattern generally indexed with respect to an hexagonal cell of $a = 0.36$ nm and $c = 1.1$ nm, where the main peaks correspond to $d_{001} \sim 1.1$ nm, $d_{002} \sim 0.55$ nm and $d_{003} \sim 0.365$ nm.

4. Conclusions

Zero-valent iron barriers can be used for the decontamination of acidic leachates generated at active or abandoned mining and wastes disposal sites and loaded with low and high concentration of hazardous metal ions and sulfate. Iron reactivity is maintained over long periods, especially when the flow of the leachates is relatively low.

The main clean up mechanisms, as derived from experimental data and geochemical simulations, involve redox reactions for cadmium and copper and precipitation as metal hydroxides for aluminum, manganese, nickel, cobalt and zinc. Metal and sulfate uptake by green rust, formed by the oxidation of Fe^0 filings to $Fe^{2+}$and Fe^{3+} and confirmed by XRD analysis, may be another important clean up mechanism. Heavy metal ions may be also removed by adsorption or co-precipitation onto the iron surface and its corrosion products; this mechanism though defines the finite clean up efficiency of the system. Microbial activity, detected in the lower parts of the low-flow rate column system, enhances metal removal.

The factors that assess the long term performance of this technology include corrosion of the iron metal, potential microbial activity, precipitation of secondary phases on reactive sites and subsequent reduction of the active surface area, development of preferential flow and clogging.

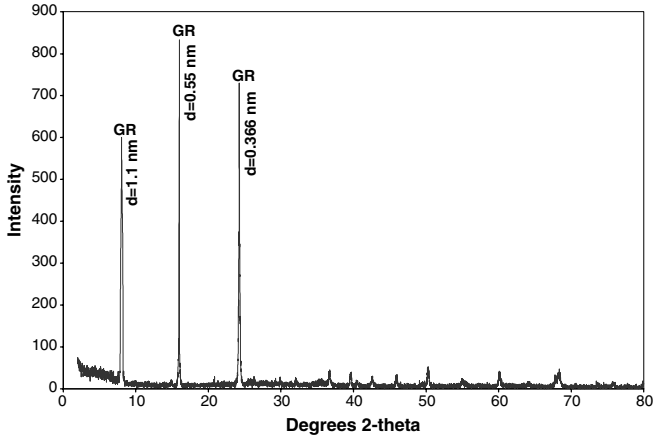

Fig. 12. X-ray diffraction pattern of precipitates formed in the LCSF column system.

Acknowledgements

The authors would like to acknowledge the financial support of the European Commission, under the "IN-TREAT" Program, INCO-CT-2003-509167.

References

Alowitz, M.J., Scherer, M.M., 2002. Kinetics of nitrate, nitrite, and Cr(VI) reduction by iron metal. Environmental Science and Technology 36 (3), 299–306.

Astrup, T., Stipp, S.L.S., Christensen, T.H., 2000. Immobilization of chromate from coal fly ash leachate using an attenuating barrier containing zero-valent iron. Environmental Science and Technology 34, 4163–4168.

Ball, J.W., Nordstrom, D.K., 1991. WATEQ4F—User's Manual With Revised Thermodynamic Data Base and Test Cases for Calculating Speciation of Major, Trace and Redox Elements in Natural Waters, US Geological Survey Open File Report, pp. 90–129.

Blowes, D.W., Ptacek, C.J., Benner, S.G., McRae, C.W.T., Bennet, T.A., Puls, R.W., 2000. Treatment of inorganic contaminants using permeable reactive barriers. Journal of Contaminant Hydrology 45, 123–137.

Brady, K., Michael, B.C., Smith, W., Schueck, J., 1998. Coal Mine Drainage Prediction and Pollution Prevention in Pennsylvania. Department of Environmental Protection, Pennsylvania.

Cantrell, K.J., Kaplan, D.I., Wietsma, T.W., 1995. Zero-valent iron for the in situ remediation of selected metals in groundwater. Journal of Hazardous Materials 42, 201–212.

Cornell, R.M., Schwertmann, U., 1996. The Iron Oxides. VCH Publishers, New York.

Domenico, P.A., Schwartz, F.W., 1998. Physical and Chemical Hydrogeology, second ed. Wiley, New York.

Furukawa, Y., Kim, J.W., Watkins, J., Wilkin, R.T., 2002. Formation of ferrihydrite and associated iron corrosion products in permeable reactive barriers of zero-valent iron. Environmental Science and Technology 36 (24), 5469–5475.

Gavaskar, A.R., Gupta, N., Sass, B.M., Janosy, R.J., O'Sullivan, D., 1998. Permeable Barriers for Groundwater Remediation; Design, Construction and Monitoring. Battelle Press, Ohio.

Génin, J.-M.R., Olowe, A.A., Refait, Ph., Simon, L., 1996. On the stoichiometry and Pourbaix diagram of Fe(II)–Fe(III) hydroxy-sulphate or sulphate-containing green rust 2. Corrosion Science 38, 1751–1762.

Gu, B., Watson, D.B., Wu, L., Phillips, D.H., White, D.C., Zhou, J.Z., 2002. Microbiological characteristics in a zero-valent iron reactive barrier. Environmental Monitoring and Assessment 77 (3), 293–309.

Herbert, R.B., 2003. Zinc immobilization by zero-valent iron: surface chemistry and mineralogy of reaction products. Mineralogical Magazine 67, 1285–1298.

Kamolpornwijit, W., Liang, L., West, O.R., Moline, G.R., Sullivan, A.B., 2003. Preferential flow path development and its influence on long-term PRB performance: column study. Journal of Contaminant Hydrology 66, 161–178.

Khudenko, B.M., 1987. Mathematical models of cementation processes. Journal of Environmental Engineering 113, 681–702.

Komnitsas, K., Bartzas, G., Paspaliaris, I., 2004. Efficiency of limestone and red mud barriers: laboratory column studies. Minerals Engineering 17, 183–194.

Kontopoulos, A., Komnitsas, K., Xenidis, A., Papassiopi, N., 1995. Environmental characterisation of the sulphidic tailings in Lavrion. Minerals Engineering 8 (10), 1209–1219.

Lee, T., Benson, C., Eykholt, G., 2004. Waste green sands as reactive media for groundwater contaminated with trichloroethylene. Journal of Hazardous Materials 109 (1–3), 25–36.

Mayer, U., 1999. A numerical model for multicomponent reactive transport in variably saturated porous media. Ph.D. Thesis Department of Earth Sciences, University of Waterloo, Waterloo, Ontario, Canada.

Miehr, R., Tratnyek, P.G., Bandstra, J.Z., Scherer, M.M., Alowitz, M., Bylaska, E.J., 2004. Diversity of contaminant reduction reactions by zero-valent iron: role of the reductate. Environmental Science and Technology 38 (1), 139–147.

Morkin, M., Devlin, J.F., Barker, J.F., Butler, B.J., 2000. In situ sequential treatment of a mixed contaminant plume. Journal of Contaminant Hydrology 45, 283–302.

O'Loughlin, E.J., Kelly, S.D., Kemner, K.M., Csencsits, R., Cook, R.E., 2003. Reduction of Ag^{I}, Au^{III}, Cu^{II}, and Hg^{II} by Fe^{II}/Fe^{III} hydroxysulfate green rust. Chemosphere 53, 437–446.

Olowe, A.A., Génin, J.-M.R., 1991. The mechanism of oxidation of ferrous hydroxide in sulfated aqueous media: importance of the initial ratio of the reactants. Corrosion Science 32, 965–984.

Park, J.-B., Lee, S.-H., Lee, J.-W., Lee, C.-Y., 2002. Lab scale experiments for permeable reactive barriers against contaminated groundwater with ammonium and heavy metals using clinoptilolite (01-29B). Journal of Hazardous Materials 95, 65–79.

Parkhurst, D.L., Appelo, C.A.J., 1999. User's guide to PHREEQC (version 2): A computer program for speciation, batch reaction, one-dimensional transport, and inverse geochemical calculations. US Geological Survey Water Resources Investigations, pp. 99–4259.

Phillips, D.H., Gu, B., Watson, D.B., Roh, Y., Liang, L., Lee, S.Y., 2000. Performance evaluation of a zero-valent iron reactive barrier: mineralogical characteristics. Environmental Science and Technology 34, 4169–4176.

Satapanajaru, T., Shea, P.J., Comfort, S.D., Roh, Y., 2003. Green rust and iron oxide formation influences metolachlor dechlorination during zero-valent iron treatment. Environmental Science and Technology 37 (22), 5219–5227.

Shokes, T.E., Möller, G., 1999. Removal of dissolved heavy metals from acid rock drainage using iron metal. Environmental Science and Technology 33, 282–287.

Su, C., Puls, R., 2001. Arsenate and arsenite removal by zero-valent iron: kinetics, redox transformation, and implications for in situ groundwater remediation. Environmental Science and Technology 35 (7), 1487–1492.

Su, C., Puls, R., 1999. Kinetics of trichloroethene reduction by zero-valent iron and tin pretreatment effect, apparent activation energy, and intermediate products. Environmental Science and Technology 33, 163–168.

USEPA, 1976. Development Document for Interim Final Effluent Limitations Guidelines and New Source Performance Standards for the Coal Mining Point Source Category. EPA 440/1-76/057a. p. 288.

Wang, C.B., Zhang, W.X., 1997. Synthesizing nanoscale iron particles for rapid and complete dechlorination of TCE and PCBs. Environmental Science and Technology 31, 2154–2156.

Westerhoff, P., 2003. Reduction of nitrate, bromate, and chlorate by zero valent iron (Fe^{0}). Journal of Environmental Engineering 129 (1), 10–16.

Wilkin, R.T., McNeil, M.S., 2003. Laboratory evaluation of zero-valent iron to treat water impacted by acid mine drainage. Chemosphere 53, 715–725.

Zhang, Y.Q., Wang, J., Amrhein, C., Frankenberger, W.T., 2005. Removal of selenate from water by zero valent iron. Journal of Environmental Quality 34, 487–495.